

DOI: 10.1002/adma.200800791

# Bioinspired Self-Cleaning Antireflection Coatings\*\*

By *Wei-Lun Min, Bin Jiang, and Peng Jiang\**

Millions of years before we began to generate functional nanostructures, biological systems were using nanometer-scale architectures to produce unique functionalities.<sup>[1–3]</sup> For instance, moths use hexagonal arrays of nonclose-packed (ncp) nipples as antireflection coatings (ARCs) to reduce reflectivity from their compound eyes.<sup>[1,3,4]</sup> The outer surface of the corneal lenses of moths consists of ncp arrays of conical protuberances, termed corneal nipples, typically of sub-300 nm height and spacing.<sup>[4]</sup> These arrays of subwavelength nipples generate a graded transition of refractive index, leading to minimized reflection over a broad range of wavelengths and angles of incidence.<sup>[5]</sup> Similar periodic arrays of ncp pillars have also been observed on the wings of cicada to render superhydrophobic surfaces for self-cleaning functionality.<sup>[2]</sup> In this Communication, we report a simple and scalable bioinspired templating technique for fabricating broadband and superhydrophobic ARCs on technologically important silicon and glass substrates.

Crystalline silicon is the most important material for solar cells.<sup>[6,7]</sup> Unfortunately, due to the high refractive index of silicon, more than 30% of incident light is reflected back from the surface of crystalline silicon.<sup>[6]</sup> ARCs are therefore widely utilized to reduce the unwanted reflective losses. Quarter-wavelength silicon nitride ( $\text{SiN}_x$ ) films deposited by plasma-enhanced chemical vapor deposition (PECVD) are the industrial standard for ARCs on crystalline silicon substrates.<sup>[8]</sup> However, the PECVD-deposited  $\text{SiN}_x$  films are expensive to fabricate. Additionally, commercial  $\text{SiN}_x$  ARCs are typically designed to suppress reflection efficiently at wavelengths around 600 nm.<sup>[6]</sup> The reflective loss is rapidly increased for near-infrared and other visible wavelengths, which contain a large portion of the incident solar energy. In contrast, subwavelength-structured moth-eye ARCs directly patterned in the substrates are broadband and intrinsically more stable and durable than multilayer ARCs since no foreign material is involved.<sup>[9–12]</sup> Nevertheless, current top-down lithographic technologies in creating subwavelength

silicon gratings, such as electron-beam lithography,<sup>[13,14]</sup> nanoimprint lithography,<sup>[15]</sup> and interference lithography,<sup>[12]</sup> require sophisticated equipment and are expensive to implement.

Glass is another important optical substrate. Although the reflective loss from glass is not as severe as that from silicon, a ca. 4% optical reflection from each air/glass interface could still degrade the performance of optical devices especially when multiple components are involved.<sup>[16,17]</sup> To generate efficient ARCs on glass substrates, various bottom-up self-assembly techniques have been extensively exploited.<sup>[18–28]</sup> For instance, layer-by-layer assembly of polyelectrolyte or polyelectrolyte–colloid multilayers has been demonstrated as an efficient means in creating ARCs on glass.<sup>[16,18,22,26]</sup> Unfortunately, traditional bottom-up techniques suffer from low throughput and incompatibility with standard microfabrication, limiting the mass production of practical coatings. Furthermore, only limited, close-packed crystal structures are available through conventional colloidal self-assemblies, whereas ncp structures are needed to mimic the microstructures on natural moth eyes and cicada wings.<sup>[4]</sup>

We have recently developed several simple colloidal templating approaches for fabricating moth-eye ARCs on both glass and silicon substrates.<sup>[29–32]</sup> All these approaches are based on a simple and scalable spin-coating technique that enables wafer-scale production of colloidal crystals with ncp structures.<sup>[33,34]</sup> Although transparent polymer moth-eye ARCs with good antireflective properties has been demonstrated,<sup>[29]</sup> the low aspect ratio (ca. 0.5) of the templated nipples hampers the realization of superhydrophobic coatings.<sup>[30]</sup> Broadband silicon ARCs have been fabricated by using 2D ncp colloidal crystal as etching mask during an  $\text{SF}_6$  reactive ion etching (RIE) process.<sup>[31]</sup> However, reproducible production of wafer-scale silicon pillars with high aspect ratio ( $\geq 5.0$ ) for making superhydrophobic ARCs is difficult to achieve. Here we systematically investigate the antireflective and nonwetting properties of templated pillar arrays with high aspect ratio (up to ca. 10) to ultimately realize self-cleaning broadband ARCs on both silicon and glass substrates.

The outline of the templating procedures for patterning subwavelength pillar arrays on silicon substrates is shown in Figure 1. The spin-coating technique<sup>[34]</sup> is firstly used to generate ncp colloidal monolayers of hexagonally ordered silica particles on (100) silicon wafers (Fig. 1A). These particles are then used as etching mask during a chlorine-RIE process (5 mTorr pressure (1 Torr =  $1.333 \times 10^2$  Pa), 20 SCCM chlorine flow rate, and 80 W). As the etching rate of silica is much lower than that of silicon under above RIE conditions,<sup>[35]</sup> silica particles protect silicon immediately underneath them from

[\*] Prof. P. Jiang, W. L. Min  
Department of Chemical Engineering  
University of Florida  
Gainesville, FL 32611-6005 (USA)  
E-mail: pjiang@che.ufl.edu

Prof. B. Jiang  
Department of Mathematics and Statistics  
Portland State University  
Portland, OR 97201-0751 (USA)

[\*\*] This work was supported in part by the NSF under Grant no. CBET-0651780 and CBET-0744879, the start-up funds from the University of Florida, and the UF Research Opportunity Incentive Seed Fund.

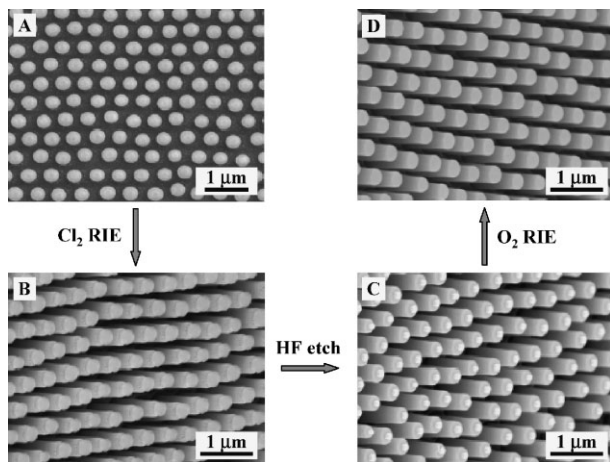


**Figure 1.** Outline of the templating procedures for fabricating antireflective silicon pillar arrays by using ncp colloidal monolayer as template.

being etched, resulting in the formation of pillar arrays directly on silicon surface (Fig. 1B). Once the silicon pillars are deep enough, the templating silica spheres can be removed by dissolving in a 2% hydrofluoric acid aqueous solution. Interestingly, we observe arrays of “micro-candles” consisting of silicon columns as candle bodies and polymer dots as candle wicks (Fig. 1C). The polymer dots are unetched residue of the thin polymer wetting layer (~100 nm thick) between the spin-coated colloidal monolayer and the silicon substrate. These dots can be easily removed by brief oxygen RIE to generate clean silicon pillar arrays (Fig. 1D).

The residual polymer dots play a crucial role in determining the shape and aspect ratio of the templated silicon pillar arrays. This accounts for the poor reproducibility and low aspect ratio of pillars generated by the SF<sub>6</sub> RIE process (40 mTorr pressure, 26 SCCM SF<sub>6</sub>, 5 SCCM O<sub>2</sub>, 25 W). In SF<sub>6</sub> RIE, reactive oxygen is also an active component that gradually attacks the polymer dots underneath the templating silica particles. When the dots are too narrow to support the silica spheres, they fall down before the silicon pillars reach enough depth. Once particle array collapses, isotropic etching of the exposed silicon pillars further reduces the aspect ratio. In contrast, during the current chlorine RIE process, reactive chlorine ions do not affect the polymer dots. This leads to the formation of silicon pillars with high aspect ratio, which benefits both antireflective and superhydrophobic properties.<sup>[2,4]</sup>

The current templating technique can be easily utilized to generate wafer-scale silicon pillar arrays. Figure 2A shows a photograph of a 4 in. silicon wafer with the right half covered by subwavelength pillars and the left half unetched. The intact left side is mirror-like and highly reflective, while the right side with moth-eye microstructures exhibits much lower reflection. This is confirmed by the appearance of the overhead lamp used to illuminate the wafer on the left side, while no reflection image is visible on the right side. Figure 2B and C show scanning electron microscope (SEM) images of silicon pillar arrays etched for 10 and 50 min, respectively. It is apparent that the templated nipples are hexagonally ordered. The

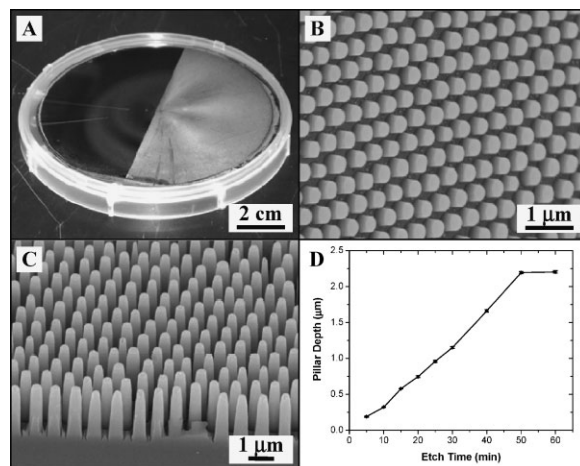


**Figure 2.** Templated silicon pillar arrays. A) Photograph of a 4 in. silicon wafer with the right half covered by subwavelength pillars and the left half unetched. The sample is illuminated with white light. B) Silicon pillars after 10 min RIE. C) Silicon pillars after 50 min RIE. D) Pillar depth dependence on RIE duration.

10 min-etched pillars have vertical sidewalls, while the 50 min-etched pillars are tapered. This is caused by the gradual shrinkage of the templating silica spheres during the RIE process. The templated pillar depths at different RIE durations are measured by cross-sectional SEM images and are shown in Figure 2D. Pillars with depth of ca. 2.2 μm and aspect ratio of ca. 10 can be reached. Longer etching results in damaged pillars due to the significant shrinkage of the templating silica spheres which are too small to protect the underneath silicon from being etched.

The specular optical reflectivity of the templated silicon pillar arrays are evaluated using visible-near-IR reflection measurement at normal incidence. The solid lines in Figure 3 show the measured reflection from a bare silicon wafer and a 60 min-etched silicon pillar array. The wafer exhibits >30% reflectivity for all above wavelengths, consistent with previous measurements.<sup>[14,23]</sup> The templated subwavelength grating

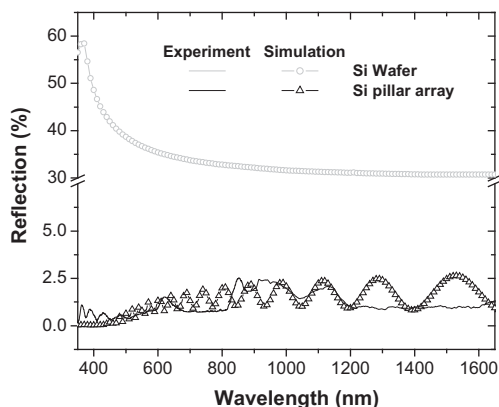


**Figure 3.** Experimental (solid) and RCWA-simulated (dotted) specular reflection at normal incidence from a flat silicon wafer and a 60 min etched silicon pillar array.

exhibits much lower reflection (<2.5%) over the whole spectrum, indicating broadband antireflection. For pillars with lower aspect ratio, the reflection increases but is always below the value of a flat silicon wafer.

The experimental reflection measurements are complemented by theoretical calculations using a rigorous coupled-wave analysis (RCWA) model.<sup>[36,37]</sup> We assume the templated pillars as shown in Figure 2D have shape like inverted circular paraboloid with base radius  $r$  and height  $h$ . We firstly divide the whole inverted circular paraboloid into 100 horizontal circular layers. The  $z$ -coordinate  $z^*$  and the radius  $r^*$  of each layer satisfy  $r^* = r\sqrt{1 - (z^*/h)^2}$ , where  $0 \leq z^* \leq h$ . The internipple distance is defined as  $\sqrt{2D}$ , where  $D$  is the diameter of templating silica spheres.<sup>[33,34]</sup> We can then calculate the fraction of silicon in each layer as  $f(z^*) = \pi(r^*)^2 / \sqrt{3}D^2$ . The effective refractive index  $n(z^*)$  of the layer at height  $z^*$  can be approximated by  $n(z^*) = \{f(z^*)n_{\text{Si}}^q + [1 - f(z^*)]n_{\text{air}}^q\}^{1/q}$ , where  $q = 2/3$ .<sup>[4,38]</sup> The complex refractive index of silicon is used to calculate the reflectance.<sup>[39]</sup> We finally calculate the reflectance of the whole system by solving the Maxwell equation to express the electromagnetic (EM) field in each layer and then matching EM boundary conditions between neighboring layers for the determination of the reflectance of the system.

The dotted lines in Figure 3 show the simulated specular reflection from a flat silicon wafer and a hexagonal array of silicon pillars with 2200 nm height templated from 380 nm silica spheres. It is apparent that the calculated reflection from the silicon wafer is very close to the measured spectrum. The simulated reflection from the templated pillar array also agrees reasonably well with the experimental spectrum, though the matching is not as good as the flat wafer. This is due to the limitation of the RCWA model which assumes a uniform refractive index instead of periodic modulation within each sliced layer.<sup>[37]</sup>

The templated silicon pillars with high aspect ratio can be used as second-generation templates to replicate polymer or glass moth-eye ARCs on transparent substrates. A poly(dimethylsiloxane) (PDMS) mold is firstly cast over the silicon template and then put on top of sol-gel glass precursor supported by a glass slide.<sup>[40]</sup> The precursor is then solidified by baking at 120 °C for 5 min. Glass pillar arrays with high aspect ratio can then be made after peeling off the PDMS mold. Figure 4 shows top- and side-view SEM images of the resulting glass pillars templated from a 30 min etched silicon pillar array. It is evident that the long-range hexagonal ordering and the interpillar distance are retained throughout the templating process. The size and depth of the glass pillars are reduced by ca. 10% than those of silicon pillars due to the volume shrinkage during the solidification of sol-gel precursor. The templated glass pillar arrays with high aspect ratio exhibit excellent antireflective properties over the whole visible spectrum (Fig. 5). The featureless glass substrate shows ca. 4% reflection for the visible spectrum, while the

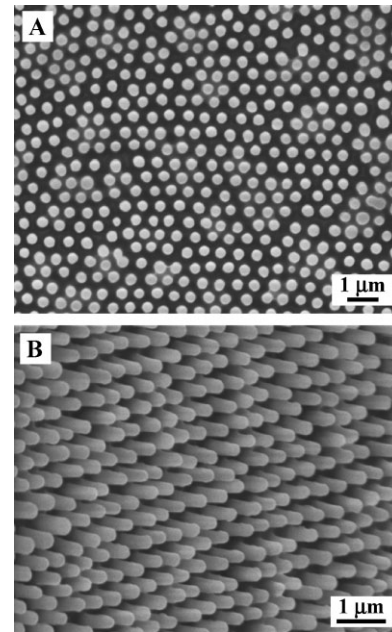


**Figure 4.** Sol-gel glass pillar array templated from a silicon pillar array (30 min RIE). A) Top-view SEM image. B) Tilted-view (45°) SEM image.

subwavelength glass pillar-covered substrate exhibits much reduced reflection (<0.5%). The simulated spectra agree reasonably well with the optical measurements for both flat glass substrate and the glass pillar array.

The templated silicon and glass subwavelength pillar arrays with high aspect ratio can also significantly enhance the hydrophobicity of the substrate surface due to the high fraction of air trapped in the trough area between pillars.<sup>[2,41,42]</sup> The hydrophobicity of silicon and glass pillars can be further improved by functionalizing them with fluorosilane through the well-established silane coupling reaction.<sup>[43]</sup> Figure 6A and B show water drop profiles on fluorosilane-modified silicon and glass pillar arrays, respectively. Both coatings are super-

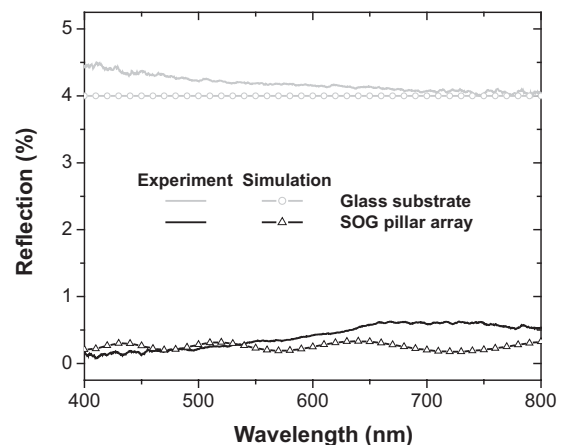


**Figure 5.** Experimental (solid) and RCWA-simulated (dotted) specular reflection at normal incidence from a flat glass substrate and a spin-on glass (SOG) pillar array as shown in Figure 4.

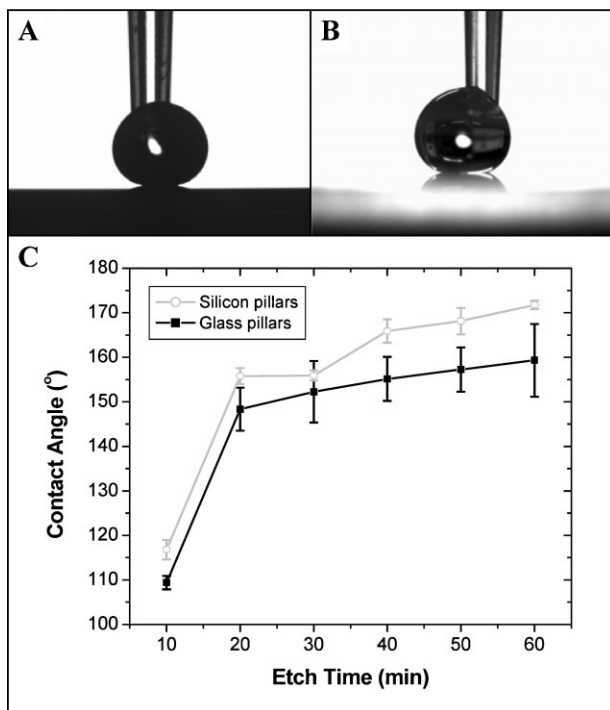


**Figure 6.** Superhydrophobic coatings achieved on both templated silicon and sol-gel glass pillar arrays. A) Water drop profile on a fluorosilane-modified silicon pillar array (60 min RIE). B) Water drop profile on a fluorosilane-modified glass pillar array templated from the sample in (A). C) Apparent water CA of templated silicon and glass pillar arrays etched at different RIE durations.

hydrophobic and the measured apparent water contact angle (CA) is ca. 172° for the former and ca. 160° for the latter, significantly enhanced from ca. 108° to ca. 105° on fluorinated flat silicon and glass substrates. Figure 6C shows the dependence of the measured water CA on RIE duration. It is apparent that longer etching duration leads to more hydrophobic surface. This agrees well with previous studies on microstructure-induced dewetting.<sup>[2,41,42]</sup> The volume shrinkage during the sol-gel glass solidification process could explain the reduced CA for glass pillar arrays than the corresponding silicon arrays.

In summary, we have developed a simple and scalable templating technique for making subwavelength ARCs on silicon and glass substrates. The templated pillar arrays with high aspect ratio exhibit excellent broadband antireflection and nonwetting properties. The technique is compatible with standard industrial manufacturing and is promising for developing self-cleaning ARCs for a large variety of technological applications ranging from solar cells and photodiodes to flat panel displays and optical components.

## Experimental

**Preparation of NCP Monolayer Colloidal Crystal Templates by Spin Coating:** Monodispersed silica colloids with ca. 380 nm diameter are synthesized by the Stober method [44, 45]. The silica colloids are

purified in 200-proof ethanol (Pharmaco Products) and then redispersed in ethoxylated trimethylolpropane triacrylate monomer (ETPTA, SR 454, Sartomer). Darocur 1173 (1 wt %) (2-hydroxy-2-methyl-1-phenyl-1-propanone, Ciba-Geigy) is added as the photoinitiator. The final particle volume fraction is adjusted to ca. 19.8%. The colloidal suspension is then dispersed on a silicon wafer (test grade, n type, Wafernet). The wafer is spun at 8000 rpm for 360 s on a standard spin coater (WS-400B-6NPP-Lite Spin Processor, Laurell). The ETPTA monomer is then photopolymerized for 4 s using a Pulsed UV Curing System (RC 742, Xenon).

**Reactive Ion Etching:** Both oxygen and chlorine RIE are performed on a Unaxis Shuttlelock RIE/ICP reactive-ion etcher. To remove the polymer matrix to release the embedded silica particles, oxygen RIE operating at 40 mTorr pressure, 40 SCCM flow rate, and 100 W is carried out for 120 s. The release silica particles can then be used as etching mask during the following chlorine-RIE process operating at 5 mTorr pressure, 20 SCCM chlorine flow rate, and 80 W to generate silicon pillars. The templating silica particles are dissolved in 2% v/v hydrofluoric acid aqueous solution for 2 min. The residual polymer dots can finally be removed by the same oxygen RIE process as described above.

**Soft-Lithography-Like Replication:** The PDMS (Sylgard 184, Dow Corning) precursors are mixed and degassed and then poured over the templated silicon pillar array. After curing at 80 °C for 30 min, the solidified PDMS mold is peeled off the silicon array. A thin layer (ca. 900 nm thick) of sol-gel glass precursor (512B, Honeywell Electronic Materials) is spin-coated at 800 rpm for 60 s on a glass slide before putting on the PDMS mold. After baking at 120 °C for 5 min and peeling off PDMS, glass pillar arrays can be formed on the glass slide.

**Optical Reflection Measurement:** An HR4000 High Resolution Fiber Optic UV-vis spectrometer and an NIR-512 spectrometer (both from Ocean Optics) with reflection probes are used for reflectance measurements. A calibrated halogen light source is used to illuminate the sample and the spectrometers can scan wavelengths from 350 to 1650 nm. Absolute reflectivity is obtained as ratio of the sample spectrum and the reference spectrum. The reference spectrum is the optical density obtained from an aluminum-sputtered (1000 nm thickness) silicon wafer. Final value of absolute reflectivity is the average of several measurements obtained from different spots on the sample surface. The resulting reflectivity is calibrated using an Ocean Optics STAN-SSL low-reflectivity specular reflectance standard for templated pillar arrays and glass slides and an STAN-SSH High-reflectivity specular reflectance standard for flat silicon wafers.

**Surface Modification and CA Measurement:** Both silicon and glass pillar arrays are chemically modified by reacting with a  $4.4 \times 10^{-3}$  M solution of (heptadecafluoro-1,1,2,2-tetrahydrodecyl) trichlorosilane (Gelest) in hexane/CCl<sub>4</sub> (v/v 70:30) for 2 h at room temperature. The resulting surfaces are rinsed with dichloromethane and ethanol and then dried under air. The apparent water CA is measured using a goniometer (NRL C.A. Goniometer, Ramé-Hart, Inc.) with autopi-petting and imaging systems.

**SEM:** SEM is carried out on a JEOL 6335F FEG-SEM. A thin layer of gold is sputtered onto the samples prior to imaging.

Received: March 20, 2008  
Revised: May 10, 2008  
Published online:

- [1] M. Srinivasarao, *Chem. Rev.* **1999**, 99, 1935.
- [2] T. L. Sun, L. Feng, X. F. Gao, L. Jiang, *Acc. Chem. Res.* **2005**, 38, 644.
- [3] P. Vukusic, J. R. Sambles, *Nature* **2003**, 424, 852.
- [4] D. G. Stavenga, S. Foletti, G. Palasantzas, K. Arikawa, *Proc. R. Soc. B* **2006**, 273, 661.
- [5] P. B. Clapham, M. C. Hutley, *Nature* **1973**, 244, 281.

- [6] *Handbook of Photovoltaic Science and Engineering*, (Eds: A. Luque, S. Hegedus), John Wiley & Sons, Chichester **2003**.
- [7] *Thin Films Solar Cells: Fabrication, Characterization and Applications*, (Eds: J. Poortmans, V. Arkhipov), John Wiley & Sons, Chichester **2006**.
- [8] P. Doshi, G. E. Jellison, A. Rohatgi, *Appl. Opt.* **1997**, *36*, 7826.
- [9] S. Chattopadhyay, L. C. Chen, K. H. Chen, *Crit. Rev. Solid State Mater. Sci.* **2006**, *31*, 15.
- [10] Y. F. Huang, S. Chattopadhyay, Y. J. Jen, C. Y. Peng, T. A. Liu, Y. K. Hsu, C. L. Pan, H. C. Lo, C. H. Hsu, Y. H. Chang, C. S. Lee, K. H. Chen, L. C. Chen, *Nat. Nanotechnol.* **2007**, *2*, 770.
- [11] Y. Kanamori, K. Hane, H. Sai, H. Yugami, *Appl. Phys. Lett.* **2001**, *78*, 142.
- [12] P. Lalanne, G. M. Morris, *Nanotechnology* **1997**, *8*, 53.
- [13] Y. Kanamori, K. Kobayashi, H. Yugami, K. Hane, *Jpn. J. Appl. Phys.* **2003**, *42*, 4020.
- [14] Y. Kanamori, M. Sasaki, K. Hane, *Opt. Lett.* **1999**, *24*, 1422.
- [15] Z. N. Yu, H. Gao, W. Wu, H. X. Ge, S. Y. Chou, *J. Vac. Sci. Technol. B* **2003**, *21*, 2874.
- [16] J. Hiller, J. D. Mendelsohn, M. F. Rubner, *Nat. Mater.* **2002**, *1*, 59.
- [17] U. Schulz, *Appl. Opt.* **2006**, *45*, 1608.
- [18] F. C. Cebeci, Z. Z. Wu, L. Zhai, R. E. Cohen, M. F. Rubner, *Langmuir* **2006**, *22*, 2856.
- [19] A. Gombert, B. Blasi, C. Buhler, P. Nitz, J. Mick, W. Hossfeld, M. Niggemann, *Opt. Eng.* **2004**, *43*, 2525.
- [20] A. Gombert, W. Glaubitt, K. Rose, J. Dreiholz, B. Blasi, A. Heinzl, D. Sporn, W. Doll, V. Wittwer, *Thin Solid Films* **1999**, *351*, 73.
- [21] M. Ibn-Elhaj, M. Schadt, *Nature* **2001**, *410*, 796.
- [22] D. Lee, M. F. Rubner, R. E. Cohen, *Nano Lett.* **2006**, *6*, 2305.
- [23] B. G. Prevo, E. W. Hon, O. D. Velev, *J. Mater. Chem.* **2007**, *17*, 791.
- [24] B. G. Prevo, Y. Hwang, O. D. Velev, *Chem. Mater.* **2005**, *17*, 3642.
- [25] S. Walheim, E. Schaffer, J. Mlynek, U. Steiner, *Science* **1999**, *283*, 520.
- [26] X. T. Zhang, O. Sato, M. Taguchi, Y. Einaga, T. Murakami, A. Fujishima, *Chem. Mater.* **2005**, *17*, 696.
- [27] H. Jiang, K. Yu, Y. C. Wang, *Opt. Lett.* **2007**, *32*, 575.
- [28] Y. Zhao, J. S. Wang, G. Z. Mao, *Opt. Lett.* **2005**, *30*, 1885.
- [29] N. C. Linn, C. H. Sun, P. Jiang, B. Jiang, *Appl. Phys. Lett.* **2007**, *91*, 101108.
- [30] C. H. Sun, A. Gonzalez, N. C. Linn, P. Jiang, B. Jiang, *Appl. Phys. Lett.* **2008**, *92*, 051107.
- [31] C. H. Sun, P. Jiang, B. Jiang, *Appl. Phys. Lett.* **2008**, *92*, 061112.
- [32] C. H. Sun, W. L. Min, N. C. Linn, P. Jiang, B. Jiang, *Appl. Phys. Lett.* **2007**, *91*, 231105.
- [33] P. Jiang, M. J. McFarland, *J. Am. Chem. Soc.* **2004**, *126*, 13778.
- [34] P. Jiang, T. Prasad, M. J. McFarland, V. L. Colvin, *Appl. Phys. Lett.* **2006**, *89*, 011908.
- [35] M. J. Madou, *Fundamentals of Microfabrication: The Science of Miniaturization*, CRC Press, Boca Raton, FL **2002**.
- [36] M. G. Moharam, T. K. Gaylord, *J. Opt. Soc. Am.* **1981**, *71*, 811.
- [37] M. G. Moharam, D. A. Pomett, E. B. Grann, T. K. Gaylord, *J. Opt. Soc. Am. A* **1995**, *12*, 1077.
- [38] H. A. Macleod, *Thin-Film Optical Filters*, Institute of Physics Publishing, Bristol **2001**.
- [39] M. A. Green, M. Keevers, *Progress Photovoltaics* **1995**, *3*, 189.
- [40] Y. N. Xia, G. M. Whitesides, *Angew. Chem, Int. Ed.* **1998**, *37*, 551.
- [41] C. W. Guo, L. Feng, J. Zhai, G. J. Wang, Y. L. Song, L. Jiang, D. B. Zhu, *ChemPhysChem* **2004**, *5*, 750.
- [42] H. Nakae, R. Inui, Y. Hirata, H. Saito, *Acta Mater.* **1998**, *46*, 2313.
- [43] Y. Coffinier, S. Janel, A. Addad, R. Blossey, L. Gengembre, E. Payen, R. Boukherroub, *Langmuir* **2007**, *23*, 1608.
- [44] W. Stober, A. Fink, E. Bohn, *J. Colloid Interface Sci.* **1968**, *26*, 62.
- [45] P. Jiang, J. F. Bertone, K. S. Hwang, V. L. Colvin, *Chem. Mater.* **1999**, *11*, 2132.